Ultrasound Tomography With Fixed Linear Arrays of Transducers

F. Natterer
Institut für Numerische und Angewandte Mathematik
Westf. Wilhelms-Universität Münster
Einsteinstrasse 62, D-48149 Münster, Germany
e-mail: nattere@math.uni-muenster.de

September 2004

1 Introduction

We consider an ultrasound scanner that consists of fixed parallel transducer arrays that are either linear (for the 2D problem) or planar (for the 3D problem); see Fig. 1. The transducers can act as sources and as receivers. The scanner can work in transmission mode and in reflection mode. In transmission mode the object to be imaged is sitting between two transducer arrays, in reflection mode on one side of two transducers. Of course we can combine transmission and reflection data to get a full data set.

The function f defining the object is

$$f = \frac{c_0^2}{c^2} - 1 - \frac{i}{k}\frac{2\alpha c_0}{c} \tag{1.1}$$

where c is the local speed of sound, $c = c_0$ outside the object constant, and α is the attenuation. $k = \omega/c_0$ is the wave number. We assume $f(x)$ to vanish outside the strip $|x_n| < R$. The transducer arrays are assumed to be perpendicular to the x_n-axis and to lie outside that strip. This means that the receiver and source arrays are of the form $(r', r_n), (s', s_n)$, respectively with $r', s' \in \mathbb{R}^{n-1}$ and $|r_n|, |s_n| \geq R$.

We model ultrasound tomography by the Helmholtz equation

$$-\Delta u - k^2(1+f)u = \delta(x-s) \tag{1.2}$$

where u is the pressure and s the source position. Upon setting

$$u(s) = G_k(x-s) + v$$

with G_k the fundamental solution of $-\Delta - k^2$ in $\mathbb{R}^n$, i. e.

$$\begin{aligned} G_k(x) &= \frac{e^{ik|x|}}{4\pi|x|} \quad \text{for } n=3, \\ G_k(x) &= \frac{i}{4} H_0(k|x|) \quad \text{for } n=2 \end{aligned}$$

we obtain

$$\Delta v(x) + k^2(1-f(x))v(x) = -k^2 G_k(x-s)f(x). \tag{1.3}$$

This differential equation has to be complemented by the Sommerfeld radiation condition at infinity. We assume $v(r)$ to be measured for each receiver r at the receiver array(s) and for each source s on the source array(s). The problem is to recover f.

First we solve the problem within the Born approximation. This is done by adjusting the method developed by Devaney [1] for plane wave irradiation to our geometry. Based on this result we determine the possible resolution and compute the point spread function for the linearized problem.

2 The Born approximation

The Born approximation is derived by neglecting the term fv on the left hand side of (1.3), obtaining

$$\Delta v(x) + k^2 v(x) = -k^2 G_k(x-s)f(x). \tag{2.1}$$

With the help of the fundamental solution G_k this can be written as

$$v(r) = k^2 \int G_k(r-x)f(x)G_k(x-s)dx \tag{2.2}$$

for each receiver r. For each $x \in \mathbb{R}^n$ we put

$$x = \begin{pmatrix} x' \\ x_n \end{pmatrix} \ , \ x' \in \mathbb{R}^{n-1}$$

and correspondingly for r, s. With $g(r,s) = v(r)$ the data function we can rewrite (2.2) as

$$g_k(r', r_n, s', s_n) = k^2 \int_{-R}^{R} \int_{\mathbb{R}^{n-1}} G_k(r' - x', r_n - x_n) f(x', x_n) G_k(x' - s', x_n - s_n) dx' dx_n \quad (2.3)$$

Following [1] we now make use of the plane wave decomposition of G_k, to wit

$$G_k(x) = ic_n \int_{\mathbb{R}^{n-1}} e^{i(|x_n| a(z) - x' \cdot z)} \frac{dz}{a(z)}, \quad (2.4)$$

$$c_2 = \frac{1}{4\pi} \ , \ c_3 = \frac{1}{8\pi^2}, a(z) = \sqrt{k^2 - z^2};$$

see [2], p. 49. Since $|r_n|, |s_n| \geq R$ we have for $x_n \in [-R, R]$ with $\epsilon_r = sgn\, r_n$, $\epsilon_s = sgn\ s_n$ the relations $|r_n - x_n| = \epsilon_r (r_n - x_n)$, $|x_n - s_n| = \epsilon_s (s_n - x_n)$.

Hence inserting (2.4) into (2.3) yields

$$g_k(r', r_n, s', s_n) = -c_n^2 k^2 \int_{-R}^{R} \int_{\mathbb{R}^{n-1}} \int_{\mathbb{R}^{n-1}} e^{i(\epsilon_r (r_n - x_n) a(z) - (r' - x') \cdot z)} \frac{dz}{a(z)} \, f(x', x_n)$$
$$\int_{\mathbb{R}^{n-1}} e^{i(\epsilon_s (s_n - x_n) a(w) - (x' - s') \cdot w)} \frac{dw}{a(w)} \, dx' dx_n.$$

The integration with respect to x', x_n is just a Fourier transform. Thus we have

$$g_k(r', r_n, s', s_n) = -c_n^2 k^2 (2\pi)^{n/2} \int_{\mathbb{R}^{n-1}} \int_{\mathbb{R}^{n-1}}$$
$$\hat{f}\left(-z + w, \varepsilon_r \, a(z) + \varepsilon_s \, a(w)\right) e^{i(|r_n| a(z) + |s_n| a(w) - r' \cdot z + s' \cdot w)} \, \frac{dz \, dw}{a(z) a(w)} \ .$$

Multiplying by $e^{-i(r'\cdot\varrho'+s'\cdot\sigma')}$, integrating with respect to r', s', and observing that

$$(2\pi)^{1-n} \int\limits_{\mathrm{R}^{n-1}} e^{-ir'\cdot\varrho'} dr' = \delta(\varrho')$$

we obtain for the (2n-2)-dimensional Fourier transform of $g(r', r_n, s', s_n)$ with respect to r', s'

$$\begin{aligned}
\hat{g}_k(\varrho', r_n, \sigma', s_n) &= (2\pi)^{1-n} \int\limits_{\mathrm{R}^{n-1}} \int\limits_{\mathrm{R}^{n-1}} g(r', r_n, s', s_n) e^{-i(r'\cdot\varrho'+s'\cdot\sigma')}\, dr' ds' \\
&= -c_n^2 k^2 (2\pi)^{n/2} \int\limits_{\mathrm{R}^{n-1}} \int\limits_{\mathrm{R}^{n-1}} \hat{f}\left(-z+w, \epsilon_r\, a(z) + \epsilon_s\, a(w)\right) \\
&\quad e^{i(|r_n|a(z)+|s_n|a(w))}\, \delta(\varrho'+z)\delta(\sigma'-w)\, \frac{dz\, dw}{a(z)a(w)} \\
&= -c_n^2 k^2 (2\pi)^{n/2} \hat{f}(\varrho'+\sigma', \epsilon_r a(\varrho') + \epsilon_s a(\sigma')) e^{i(|r_n|a(\varrho')+|s_n|a(\sigma'))}.
\end{aligned}$$

Thus

$$\hat{f}(\varrho'+\sigma', \epsilon_r a(\varrho') + \epsilon_s a(\sigma')) = -\frac{e^{i(|r_n|a(\varrho')+|s_n|a(\sigma'))}}{c_n^2 k^2 (2\pi)^{n/2}} \hat{g}_k(\varrho', r_n, \sigma', s_n). \quad (2.5)$$

This is the solution of the ultrasound tomography problem within the Born approximation.

3 Resolution

Given the data $g_k(r', r_n, s', s_n)$ for $r', s' \in \mathbb{R}^{n-1}$ and k fixed we can determine

$$\hat{f}(\varrho'+\sigma', \epsilon_r a(\varrho') + \epsilon_s a(\sigma')), \varrho', \sigma' \in \mathbb{R}^{n-1}.$$

We consider the following modes

1. Transmission mode, i. e. $r_n \geq R, s_n \leq -R$.
   In that case $\epsilon_r = 1, \epsilon_s = -1$. Hence

   $$\hat{f}(\varrho'+\sigma', a(\varrho') - a(\sigma')), \varrho', \sigma' \in \mathbb{R}^{n-1}$$

   is determined. For $|\varrho'| < k, |\sigma'| < k$, the argument of $\hat{f}$ runs through all the semispheres (or semicircles for $n = 2$) of radius k pointing downwards whose midpoints are on the semisphere in the upper halfplane with radius k around the origin; see Fig. 2 for the case $n = 2$. For $n = 2$ these semicircles fill the two disks of radius k around $\varrho' = \pm k$.

2. Reflection mode, i. e. $r_n \leq -R, s_n \leq -R$.
   In that case $\epsilon_r = -1, \epsilon_s = -1$.

$$\hat{f}(\varrho' + \sigma', -a(\varrho') - a(\sigma')), \varrho', \sigma' \in \mathbb{R}^{n-1}$$

   is determined. Hence $\hat{f}$ is determined on all semispheres of radius k and pointing downwards whose midpoint lies on the semisphere in the lower halfplane with radius k around the origin; see Fig. 3 for the case $n = 2$. For $n = 2$ these semicircles fill the semicircle of radius $2k$ in the lower halfplane with the semicircles of radius k around $(\pm k, 0)$ removed.

   Correspondingly, if the reflection scan is done from the opposite side, i. e. $r_n \geq R, s_n \geq R$,

$$\hat{f}\left(\varrho' + \sigma', a(\varrho') + a(\sigma')\right), \varrho, \sigma' \in \mathbb{R}^{n-1}$$

   is given.

3. Combining transmission scan with reflection scans from opposite sides provides the values of $\hat{f}$ on a ball of radius $2k$ around the origin, leading to resolution of $\lambda/2$ where $\lambda = 2\pi/k$ is the wavelength of the irradiating waves. This is the resolution of plane wave irradiation from all directions.

4 Implementing the Born approximation

In principle the Born approximation can be implemented by interpolation in Fourier space. For ease of exposition we consider only the case $n = 2$. For each point ξ on a cartesian grid in the circle $|\xi| < 2k$ we have to find ϱ', σ' such that

$$\xi_1 = \varrho' + \sigma', \xi_2 = \varepsilon_r a(\varrho') + \varepsilon_s a(\sigma') \tag{4.1}$$

We distinguish 3 cases:

(i) ξ is inside one of the circles of radius k around $(\pm k, 0)$. Then $\varepsilon_r = 1, \varepsilon_s = -1$ (transmission).

(ii) ξ is outside the circles in (i) and $\xi_2 > 0$. Then $\varepsilon_r = -1, \varepsilon_s = -1$ (reflection with both sources and receivers on the bottom).

(iii) As in (ii), but $\xi_2 < 0$. Then $\varepsilon_r = 1, \varepsilon_s = 1$ (reflection with both sources and receivers on top).

Solving (4.1) for ϱ', σ' leads to

$$\sigma' = \frac{\xi_1}{2} + \frac{\xi_2}{2|\xi|}\sqrt{4k^2 - |\xi|^2} \quad , \quad \varrho' = \frac{\xi_1}{2} - \frac{\xi_2}{2|\xi|}\sqrt{4k^2 - |\xi|^2} \tag{4.2}$$

The values of $\hat{f}$ we have to assign to ϱ', σ' are

$$\hat{f}\left(\varrho' + \sigma', \varepsilon_r a(\varrho') + \varepsilon_s a(\sigma')\right) \tag{4.3}$$

with $\varepsilon_r, \varepsilon_s$ chosen according to (i), (ii) and (iii).

With (4.2), (4.3) it is easy to compute $\hat{f}$ on a cartesian grid by interpolation. Unfortunately, simple interpolation methods such as nearest neighbor are not sufficiently accurate. As a rule of thumb $\hat{g}$ has to be oversampled by a factor of 32 at least to yield a sufficiently accurate approximation to $\hat{f}$ at the grid points. By this we mean that on a $p \times p$ cartesian grid for $\hat{f}$ we need $\hat{g}$ sampled on a $32p \times 32p$ grid in $[-k, k]^2$. In most applications this is prohibitive.

A way out is the use of FFT algorithms on non-equidistant grids. Assume that $\hat{g}$ is given on the grid

$$\begin{pmatrix} h\ell \\ hm \end{pmatrix}, \ell, m = -p, \cdots, p \tag{4.4}$$

where $h = k/p$. Then $\hat{f}$ is given on the grid

$$\begin{pmatrix} h(\ell + m) \\ \varepsilon_r a(h\ell) + \varepsilon_s(hm) \end{pmatrix}, \ell, m = -p, \cdots, p \tag{4.5}$$

in the ξ_1 - ξ_2 plane, with $\varepsilon_r, \varepsilon_s$ chosen according to (i), (ii), (iii). This grid is equidistant in ξ_1 but non-equidistant in ξ_2. This is a perfect example for the non-equidistant FFT as suggested by Fourmont [3].

In Fig. 4 we display the points (4.5) for $p = 6$. The red dots correspond to case (i), the blue spots to cases (ii) and (iii). We see that the grid is strongly non-equidistant in the vertical (ξ_2) direction.

In Fig. 5 we reconstructed the function

$$f(x) = \begin{cases} 1, & |x| \leq 1, \\ 0 & \text{otherwise} \end{cases}$$

from the values of $\hat{f}$ at the points (4.5). Starting out from these values we computed approximations to $\hat{f}$ on the cartesian grid $(\ell_1, \ell_2)\pi/R, \ell_1, \ell_2 = -q, \cdots, q, q = 64, R = 2$. This is in agreement with the sampling theorem. We used nearest neighbor interpolation and piecewise linear interpolation. We display only the results of nearest neighbor interpolation since the results of piecewise linear interpolation are only slightly better.

As reference picture we display in Fig. 5(d) the reconstruction of f from the exact values of $\hat{f}$ on the cartesian grid. In Fig. 5 (a) - (c) we computed the values of $\hat{f}$ on the cartesian grid approximately by nearest neighbor interpolation from the values of $\hat{f}$ on (4.5) with $p = 256, 521, 1024$, respectively. We see that the results become better as p increases but do not reach the quality of the reference picture.

5 Backscatter

In this section we consider the case of pure backscatter, i. e. $s' = r'$ runs over $\mathbb{R}^{n-1}$ and $s_n = r_n$ fixed. In seismics this is called the zero-offset case. We follow the treatment in Bleistein et al. [5]. (2.3) assumes the form

$$g_k(r, r) = k^2 \int_{-R}^{R} \int_{\mathrm{R}^{n-1}} G_k^2(r - x) f(x) dx \tag{5.1}$$

For $n = 3$ this reads

$$g_k(r,r) = \frac{k^2}{16\pi^2} \int_{-R}^{R} \int_{\mathbf{R}^2} \frac{e^{2ik|r-x|}}{|r-x|^2}\, f(x)dx.$$

Differentiating with respect to k we obtain

$$\frac{d}{dk}\,\frac{g_k(r,r)}{k^2} \;=\; \frac{i}{2\pi^2} \int_{-R}^{R} \int_{\mathbf{R}^2} \frac{e^{2ik|r-x|}}{4\pi|r-x|}\, f(x)dx. \tag{5.2}$$

The kernel of this integral equation is just $G_{2k}(r-x)$. Using (2.4) we obtain

$$\frac{d}{dk}\,\frac{g_k(r,r)}{k^2} \;=\; \frac{-c_3}{2\pi^2} \int_{-R}^{R} \int_{\mathbf{R}^2} \int_{\mathbf{R}^2} e^{i(|r_n-x_n|a(z)-(r'-x')\cdot z)}\, \frac{dz}{a(z)}\, f(x)dx$$

where now $a(z) = \sqrt{4k^2 - z^2}$. Assuming $r_n \geq R$ we can drop the absolute value sign in the exponent, obtaining

$$\frac{d}{dk}\,\frac{g_k(r,r)}{k^2} \;=\; \frac{-c_3}{2\pi^2}\,\frac{1}{2\pi} \int_{\mathbf{R}^2} e^{i(r_n a(z)-r'\cdot z)}\, \hat{f}(z,a(z))\frac{dz}{a(z)}.$$

Multiplying by $e^{ir'\cdot w}$ and integrating with respect to w yields

$$\begin{aligned} \int_{R^2} e^{ir'\cdot w}\, \frac{d}{dk}\,\frac{g_k(r,r)}{k^2}\, dr' &= -\frac{c_3}{\pi} \int_{\mathbf{R}^2} e^{ir_n a(z)}\, \hat{f}(z,a(z))\delta(z-w)\frac{dz}{a(z)} \\ &= -\frac{c_3}{\pi}\,\frac{e^{ir_n a(w)}}{a(w)}\, \hat{f}(w,a(w)). \end{aligned} \tag{5.3}$$

Thus we see that from knowing the backscattered signal in a small frequency band around k we can determine $\hat{f}$ - within the Born approximation - on a circle of radius $2k$. If all frequencies are available, $\hat{f}$ is determined inside the ball of radius $2k$.

A different treatment of the latter case is due to Norton and Linzer [4]. Fourier transforming (5.2) with respect to k we obtain

$$\int_{\mathbf{R}^1} e^{-iks}\frac{d}{dk}\,\frac{g_k(r,r)}{k^2}\, dk \;=\; \frac{i}{2\pi^2} \int_{-R}^{R} \int_{\mathbf{R}^2} \int_{\mathbf{R}^1} e^{ik(2|r-x|-s)}\, dt\, \frac{dx}{4\pi|x-r|}$$

$$
\begin{aligned}
&= \frac{i}{\pi} \int_{-R} \int_{\mathrm{R}^2} \frac{\delta(2|r-x|-s)}{4\pi|x-r|} f(x)dx \\
&= \frac{i}{2\pi^2 s} \int_{|r-x|=s/2} f(x)dx.
\end{aligned}
$$

Thus the integrals of f over balls of arbitrary radius around r are determined.

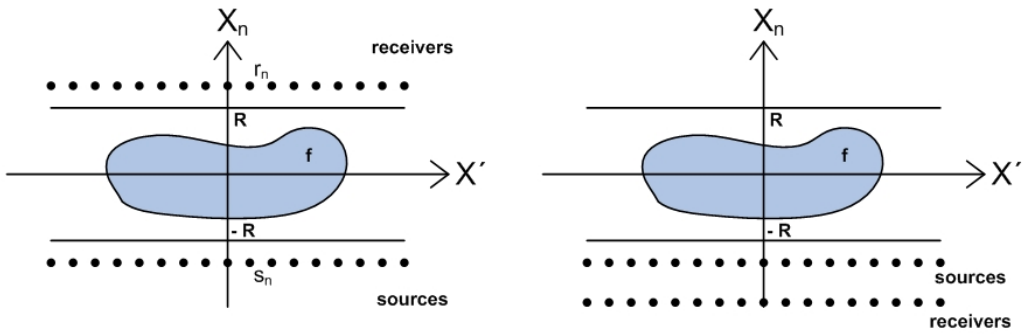

Fig. 1: Geometry of ultrasound scanner, $n = 2$. Left: Transmission mode. Right: Reflection mode.

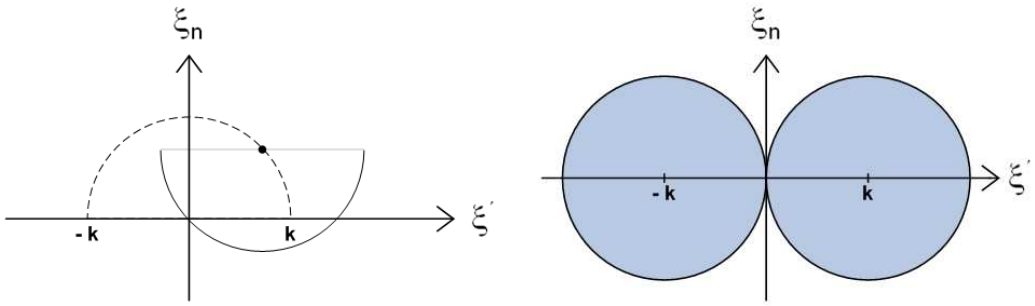

Fig. 2: Left: Semicircles (solid line) on which $\hat{f}$ is determined in transmission mode. Right: Domain that is filled by these circles

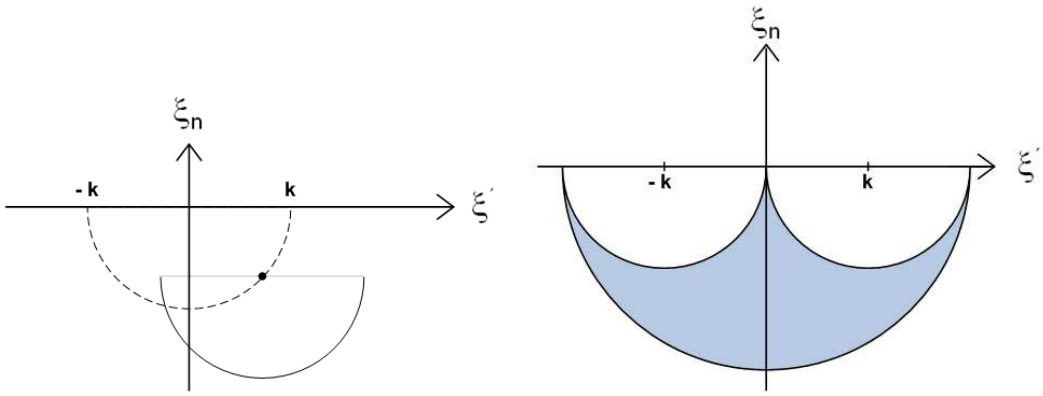

Fig. 3: Same as Fig. 2, but for reflection mode, with sources and receivers sitting below $x_n = -R$. For sources and receivers above $x_n = R$ the Figures here to be flipped around the ξ' axis.

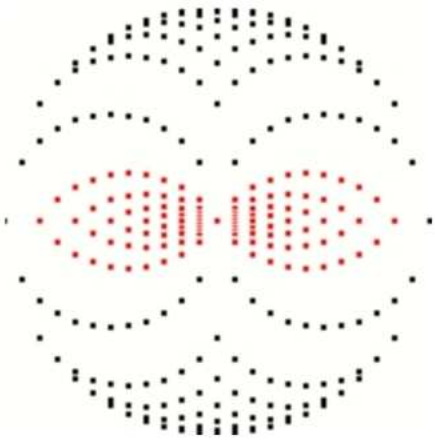

Fig. 4: Points (4.5) at which $\hat{f}$ is given. Red spots: case (i) (transmission) Blue spots: cases $(ii), (iii)$ (reflection)

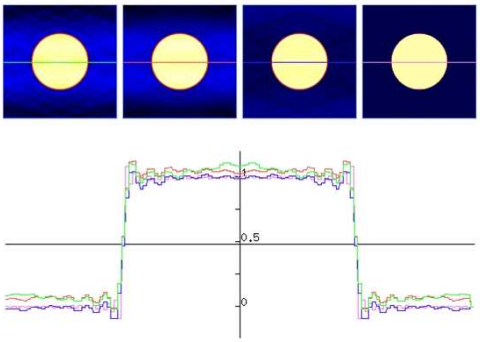

Fig. 5: Reconstruction of disk, Top (from left to right): Nearest neighbour interpolation with $p = 256, p = 512, p = 1024$, reference picture computed exact values. Bottom: Cross section along lines shown in the pictures.

References

[1] Devaney, A. J.: A filtered bachpropagation algorithem for diffraction tomography, Ultrasonic Imaging **4**, 336 - 350 (1982).

[2] Natterer, F. and Wübbeling, F.: Mathematical Methods in Image Reconstruction, SIAM 2001.

[3] Fourmont, K.: Non-equispaced fast Fourier transforms with applications to tomography, J. Fourier Anal. Appl. **9**, 431 - 450 (2003)

[4] Norton, S. J., and Linzer, M.: Ultrasonic reflectivity imaging in three dimensions: Exact inverse scattering solutions for plane, cylindrical and spherical apertures, IEEE Transaction as Biomedical Engineering, **28**, 2002 - 220 (1981).

[5] Bleistein, N., Cohen, J. K., and Stockwell (Jr.), J. W.: Mathematics of Multidimensional Seismic Imaging, Migration, and Inversion. Springer 2001